Available online at www.sciencedirect.com
SCIENCE DIRECT®
Analytical Biochemistry 337 (2005) 22–34
ANALYTICAL BIOCHEMISTRY
www.elsevier.com/locate/yabio

Analysis of connective tissues by laser capture microdissection and reverse transcriptase-polymerase chain reaction

Robin Jacquet, Jennifer Hillyer, William J. Landis*

Department of Biochemistry and Molecular Pathology, Northeastern Ohio Universities College of Medicine, Rootstown, OH 44272, USA

Received 3 June 2004

Abstract

Studies of gene expression from bone, cartilage, and other tissues are complicated by the fact that their RNA, collected and pooled for analysis, often represents a wide variety of composite cells distinct in individual phenotype, age, and state of maturation. Laser capture microdissection (LCM) is a technique that allows specific cells to be isolated according to their phenotype, condition, or other marker from within such heterogeneity. As a result, this approach can yield RNA that is particular to a subset of cells comprising the total cell population of the tissue. This study reports the application of LCM to the gene expression analysis of the cartilaginous epiphyseal growth plate of normal newborn mice. The methodology utilized for this purpose has been coupled with real-time quantitative reverse transcriptase-polymerase chain reaction (QRT-PCR) to quantitate the expression of certain genes involved in growth plate development and calcification. In this paper, the approaches used for isolating and purifying RNA from phenotypically specific chondrocyte populations of the murine growth plate are detailed and illustrate and compare both qualitative and quantitative RT-PCR results. The technique will hopefully serve as a guide for the further analysis of this and other connective tissues by LCM and RT-PCR.

Keywords: Laser capture microdissection; Real-time reverse transcriptase-polymerase chain reaction; Growth plate cartilage; Connective tissue

Laser capture microdissection (LCM)[1] was first described by Emmert-Buck et al. [1]. Since its initial use and publication, LCM has been successfully applied to investigate many different tissues by isolating specific cells from among the total heterogeneous cell population comprising them. The isolations have been performed with minimal contamination from the surrounding environment [2,3]. Bone tissue is composed of a number of regions that are functionally distinct and constituted by cells varying in phenotype, age, maturation, or other conditions or characteristics. Such heterogeneity has not been conducive to gene analysis of selective bone cell types although a number of different approaches have been attempted to resolve the situation. One approach using homogenates from whole bone or specific bone regions necessarily contains mixed cellular populations and the contribution of gene expression from a particular cell type such as chondrocytes or osteoblasts is confounded and impossible to assess. Tissue sectioning as a second approach to gene expression is more practical than homogenate analysis but it has been hindered because the typical paraffin embedding of specimens may adversely affect the integrity of the RNA [4]. Frozen tissue sectioning is a recommended alternative for RNA recovery. However, it and other RNA techniques such as in situ hybridization are problematic and challenging because bone is mechanically

* Corresponding author. Fax: +330 325 5925.
E-mail address: wjl@neoucom.edu (W.J. Landis).

[1] *Abbreviations used:* LCM, laser capture microdissection; QRT-PCR, quantitative reverse transcriptase-polymerase chain reaction; DEPC, diethylpyrocarbonate; NTC, no-template control; OPN, osteopontin.

0003-2697/$ - see front matter © 2004 Elsevier Inc. All rights reserved.
doi:10.1016/j.ab.2004.09.033

hard and its partial decalcification, which may also alter RNA, may be required as an only option. Even when operationally successful, in situ hybridization often provides poor cellular localization of gene markers and small changes in expression that are difficult to detect.

Studies reporting the use of LCM to examine gene expression in mineralized tissues are limited and involve analysis of tumor cells and bone marrow [5,6], normal and tissue-engineered teeth [7–9], growth plate cartilage [10–15], and osteoarthritis [16]. The restricted scope of application of LCM in this capacity may be attributable to a number of factors. A major difficulty with laser capture of a calcified tissue is generating a morphologically acceptable, intact section that adheres to a slide and also permits microdissection and maintenance of the integrity of its intrinsic RNA. With regard to microdissection (with the Arcturus PixCell II system as applied here), a second problem is obtaining an individual section that is flat and dry to be processed for subsequent LCM. Bone presents a unique challenge in this context since it typically contains both unmineralized and mineralized regions and their interfaces. Third, the actual capture of individual osteoblasts or chondrocytes in bone tissue is troublesome because the cells are intimately integrated within their elaborated extracellular matrix. This characteristic commonly prevents consistent cell isolations that are matrix-free or precludes any cell capture whatsoever.

This paper presents results of a variety of approaches to address each of the principal obstacles above so that LCM and gene analysis can be achieved consistently and successfully with bone and mineralized tissues in general. Thus, a methodology has been developed that couples LCM with real-time quantitative reverse transcriptase-polymerase chain reaction (QRT-PCR) to quantitate gene expression in the mineralizing growth plate of young postnatal mice. LCM was used to obtain a small homogeneous sample of captured cells, and limited numbers of gene transcripts related to bone mineralization were quantitated without RNA amplification.

Materials and methods

Tissue processing

Animals were housed in the Comparative Medicine Unit of the Northeastern Ohio Universities College of Medicine and all procedures related to the animals were approved by the Institutional Animal Care and Use Committee. The 1- to 11-day-old B6C3F1 wild-type mice (Charles River Laboratories, Wilmington, MA) were euthanized by CO_2 asphyxiation. Right and left hind tibiae were excised and immediately placed in individual sterile 15-ml tubes containing RNA*later* (Ambion, Austin, TX) at 4 °C for 1 day and according to the manufacturer's instructions. Samples were then transferred to a −20 °C freezer for long-term storage. On retrieval from storage, tibiae were briefly rinsed in ice-cold diethylpyrocarbonate (DEPC)-treated water and placed in small molds to which Tissue Freezing Medium (Research Biomedical Sciences, Durham, NC) was added. Embedded specimens were then frozen on a cold plate at −20 °C inside a Reichert HistoStat (Scientific Instruments, Buffalo, NY). Frozen tibiae were next removed from their molds and mounted onto stubs for subsequent sectioning at −20 °C. Full longitudinal sections (5–7 μm in thickness) of tibiae were cut on the HistoStat using a D-profile tungsten carbide blade. A CryoJane Tape Transfer System (Instrumedics, Hackensack, NJ) was incorporated into the HistoStat as an aid to sectioning and adhering sections to treated (1× adhesive-coated) glass slides (Instrumedics). All sections were stored in a −80 °C freezer in slide boxes containing silica gel capsules prior to laser capture.

In some experiments, excised tibiae were placed in sterile 30% sucrose [17] for comparison with RNA*later* with regard to the respective effects on gene expression and tissue morphology. Samples were soaked in sucrose for 4 h at 4 °C, frozen in liquid nitrogen-cooled isopentane (−160 °C), and then stored at −80 °C. On retrieval from storage, samples were mounted onto Histostat stubs with Tissue Freezing Medium, sectioned at −20 °C, and processed as noted for RNA*later*-preserved specimens. Sucrose-preserved sections were likewise stored at −80 °C.

Laser capture microdissection

The basic protocol outlined by the NIH (http://dir.nichd.nih.gov/lcm/lcm.htm) was used but modified as detailed below to accommodate the unique characteristics of bone as a hard connective tissue. Care was taken to maintain an RNase-free environment and all solutions were made with DEPC-treated water. Either RNA*later*- or sucrose-preserved glass-mounted sections of mouse tibia stored at −80 °C were immediately fixed for 1 min in a slide jar containing 70% ethanol. The transfer of frozen slides to ethanol was made inside the −80 °C freezer. Slides were then rinsed for 1 min at room temperature in DEPC-treated water and 1 min subsequently in 95% ethanol before staining for 30 s in alcoholic eosin (Eosin Y; EM Science, Gibbstown, NJ). Sections were subsequently dehydrated in graded ethanol solutions (95% [1×], 100% [2×]) for 1 min each and then 100% xylene [2×] for 5 min each. The fixation and staining protocol preserved RNA [4,10,11,17,18]. The sections were air dried in a fume hood for several minutes before storing them in a desiccator over Drierite (W.A. Hammond Drierite, Xenia, OH) in preparation for laser capture.

Laser capture microdissection was performed with a PixCell II laser capture system (Arcturus Engineering, Mountain View, CA). A laser spot size was selected as either 7.5 or 15 μm diameter, depending on the area of the region to be captured, with 70–80 mW power and 1.5–2.5 ms pulse duration. Individual or groups of chondrocytes comprising the cartilaginous epiphyseal growth plates of the mouse tibiae were observed and identified in objective lens fields and captured (microdissected) as described previously [14]. Captured cells were examined on the transparent polymer transfer films of Cap-Sure small cylinder caps (Arcturus Engineering) and debris or excess section material removed by gently touching the film to a piece of clean double-sided tape. From 10 to approximately 1200 cells were captured in different experiments reported below. Images of tissue sections appearing before and after cell capture and of captured cells attached to cap transfer films were recorded and stored utilizing the archiving workstation of the PixCell II system.

RNA isolation

Total RNA was isolated from both chondrocytes captured on transfer films and whole mouse bones. The latter served as control RNA for various purposes in the procedure (see below). Mouse bones were ground under liquid nitrogen and RNA was isolated with TRI Reagent (Molecular Research Center, Cincinnati, OH) following the manufacturer's protocol. The chondrocytes on transfer films were inserted into Eppendorf tubes where they were lysed from caps by inverting and vortexing the tubes for 2 min in 200 μl RNA extraction buffer (0.5% *N*-lauroylsarcosine, 0.02 M sodium citrate [pH 7.0], 4 M guanidine thiocyanate, DEPC-treated water to 50 ml) and 1.6 μl of β-mercaptoethanol. Caps were removed from Eppendorf tubes and examined microscopically with the LCM system to verify lysis of chondrocytes. Cell lysates were transferred to 1.5-ml centrifuge tubes containing 20 μl of 2 M sodium acetate, pH 4.0, and 220 μl phenol (high quality) saturated with DEPC-treated water. After vortexing the tubes for 1 min, 60 μl chloroform:isoamyl alcohol (49:1) was added and vortexing was repeated for an additional minute. Samples were next placed on ice for 15 min and centrifuged at 20,000*g* for 30 min at 4 °C to separate aqueous and organic layers. The upper aqueous layer containing RNA in each tube was removed to a new tube to which 20 μg of glycogen carrier was added. RNA was precipitated by addition and mixing of 200 μl of ice-cold 2-propanol to the solution and then kept at −80 °C for at least 1 h.

Total RNA from both the captured chondrocytes and the whole mouse bones was next separately pelleted at 20,000*g* for 30 min at 4 °C, washed with 75% ethanol, and resuspended in 13 μl of DEPC-treated water. The samples were DNase-treated to remove residual genomic DNA by making final volumes of 20 μl containing DNase (20 U), RNase inhibitor, and buffer (Takara Mirus Bio, Madison, WI), which were incubated for 2 h at 37 °C. DNase was inactivated with 1.25 mM EDTA at 65 °C for 10 min. Samples were phenol:chloroform-extracted as described above. Total RNA was precipitated by adding 20 μl of 4 M ammonium acetate and 80 μl of absolute ethanol at −80 °C for at least 1 h.

cDNA synthesis by reverse transcription

Initially each sample of total RNA isolated from either captured chondrocytes or ground mouse bones was divided into two tubes. One of the tubes contained no reverse transcriptase ("minus RT" or "−RT") and would be expected to have no PCR product so as to confirm an absence of genomic DNA. Reverse transcription, PCR, and real-time PCR reagents were supplied by Applied Biosystems (Foster City, CA). For cDNA synthesis, the following reagents were added to a final volume of 20 μl: 4 μl of 5× reaction buffer, 2 μl 25 mM $MgCl_2$, 2 μl dithiothreitol, 0.5 μl RNase inhibitor, 1 μl random hexamers, 1 μl oligo(dT) primers, and 2 μl of 10 mM dNTP mixture. All tubes were heated to 65 °C for 5 min and then allowed to cool at room temperature for 10 min. All −RT tubes received 1 μl DEPC-treated water and all other (positive) tubes received 1 μl (50 U) of Multiscribe reverse transcriptase. All reactions were incubated for 10 min at room temperature and then transferred to a 37 °C heat block for 60 min. Reactions were halted by heating to 95 °C for 5 min and cooling on ice.

Qualitative PCR

Sequences of primer pairs were designed using MacVector 6.5.3 DNA and Protein Sequence Analysis Software (Genetics Computer Group, Madison, WI). When possible, primer sequences were designed to span an intron and limit the possibility of amplifying genomic DNA. Primer sequences are listed in Table 1 and all, except for 18S rRNA (Ambion, Austin, TX), were synthesized by Sigma Genosys (The Woodlands, TX). Sequence specificities were confirmed using the BLAST program (National Center for Biotechnology Information; www.ncbi.nlm.nih.gov). Used with cDNA generated from mouse bone RNA (control cDNA), primer sets were optimized for $MgCl_2$ concentration and annealing temperature. Each final 30 μl PCR volume contained AmpliTaq Gold DNA Polymerase (Applied Biosystems), 0.2 mM for each dNTP, and 0.67 μM of the specific primers. PCR conditions were (stage 1) 95 °C for 6 min for enzyme activation, (stage 2) 40 cycles at 95 °C for 15 s, 30 s for annealing (58–62 °C depending on primers used), and 72 °C for 2 min for extension, and

Table 1
Primer sequences

Gene	GenBank Access. No.	Primer	Sequence 5′ to 3′	Product size (bp)
Gel-based PCR				
18S rRNA		Ambion QuantumRNA Classic Standards		488
Aggrecan	NM007424	F	GTCCCAGAAGCCAAGCAGTGACC	875
		R	ATGCCAGATCATCACCACACAGTCC	
Osteopontin	J04806	F	CAGACACTTTCACTCCAATC	390
		R	ACTTGTGGCTCTGATGTTCC	
QRT-PCR				
18S rRNA	X00686	F	AACGAGACTCTGGCATGCTAACTA	78
		R	CCACTTGTCCCTCTAAGAAGTTGG	
Aggrecan	NM007424	F	CACAGAGCTTGGAGGACTCAGA	81
		R	CACAGATGGCACAGACCTAA	
Osteopontin	J04806	F	AGTCTAGGAGTTTCCAGGTTTCTGAT	88
		R	TTAGACTCACCGCTCTTCATGTG	

(stage 3) 72 °C for 7 min with cooling to 4 °C on a Gene Amp PCR System 9700 (Applied Biosystems). PCR products (amplicons) were electrophoresed on 2–3% agarose gels. Ethidium bromide or SYBR Gold (Molecular Probes, Eugene, OR) nucleic acid stain was used to detect amplicons in agarose gels. Gels were scanned using a Kodak Digital Science Image Analysis System (Model 440CF, Eastman Kodak, Rochester, NY).

Primer sets were initially verified by restriction enzyme digestion of amplicon products. Visualized amplicon bands were excised and purified using Wizard PCR Preps DNA Purification System (Promega, Madison, WI). The isolated bands were digested with enzymes recognizing an appropriate site according to known amplicon sequence. Digests were carried out at 37 °C for 1 h as specified by the recommendations of the manufacturer (Takara Mirus Bio, Madison, WI). Following digestion, the products were resolved on a 3% ethidium bromide-stained agarose gel.

Real-time quantitative RT-PCR

Real-time QRT-PCR was performed using an ABI Prism 7700 Sequence Detector (Applied Biosystems). Primers were designed with Primer Express 1.0 software (Applied Biosystems) and are given in Table 1. The final sample volume for PCR for each control or experimental cDNA was 30 µl and contained SYBR Green Master Mix, sterile water, and 0.3 µM of each primer. SYBR Green Master Mix diluted 1:1 in sterile water from a 2× concentration was used as a blank to verify its purity. Buffer blanks contained all reaction components without cDNA. No-template controls (NTC) contained only primers and SYBR mix and verified any formation of primer dimers. All samples were run in triplicate or in duplicate depending on available cDNA. Quantitative PCR conditions were (stage 1) 95 °C for 10 min and (stage 2) 40 cycles at 95 °C for 15 s, 60 °C for 30 s, and 72 °C for 2 min. The final cycle (stage 3) heated products slowly to 95 °C while fluorescence measurements were used to generate a dissociation curve utilizing the software program v1.Ob1 provided by Applied Biosystems. From such melting curves, the degree of product purity was assessed. This was accomplished by confirming the presence of a single peak at the known product melting temperature and the absence of any primer dimers that may generate a peak at a lower temperature [19]. Amplicons were also electrophoresed on a 4% agarose gel to verify a single band at the appropriate molecular weight.

Triplicate or duplicate threshold cycle (C_T) values were generated for each sample and averaged, and standard deviations (one SD of the means) were calculated. The threshold cycle, C_T, is defined as the PCR cycle at which an increase in amplicon fluorescence is detected over a set baseline value. The approach taken in this study utilized the comparative C_T method for relative quantitation of gene levels of expression as outlined in User Bulletin No. 2 from Applied Biosystems [20]. This mode of analysis requires validation experiments to demonstrate that the efficiencies of target and reference genes are approximately equal. In this case, standard curves were first obtained by plotting the mean threshold cycle versus the log input concentration from dilutions over a 200-fold range (~0.1–20 ng) of control cDNA generated from RNA of ground mouse bones as noted above. Curves were analyzed by linear regression using Microsoft Excel (Microsoft, Redmond, WA) to yield curve slopes and R^2 values as measures of primer set efficiencies. Plots of ΔC_T versus log input concentration (~0.1–20 ng control cDNA) were subsequently generated to demonstrate approximately equal efficiencies of target and reference genes. ΔC_T is the average C_T of the target gene minus the average C_T of the reference gene. The absolute value of the slope of this plot should be <0.1 [20].

The reference gene utilized in this study was 18S rRNA, whose variation, based on the OD_{260} of identical quantities of total RNA from among a number of different experimental samples, was less than one C_T.

Histology

As a correlate to gene expression analysis, the morphology and development of organic and inorganic matrices in the cartilaginous epiphyseal growth plate of normal 1- to 11-day-old B6C3F1 wild-type mice were studied by histological techniques. For each mouse, histology utilized the tibia counterpart to the bone taken for laser capture microdissection and PCR. Tibiae were excised and fixed in 10% neutral-buffered formalin for at least 24 h, dehydrated, infiltrated, cleared in xylene, embedded in paraffin in a 60 °C oven, and cut into 5- to 7-μm thick sections. All sections were subsequently stained with toluidine blue, hematoxylin and eosin, von Kossa and/or Alizarin red. Sections were examined with an Olympus Model IX70-S1F2 light microscope (Olympus Optical, Japan).

Results

Histology of mouse bone and laser capture microdissection

The characteristic morphology of the tibial epiphyseal growth plate from a normal 9-day-old B6C3F1 mouse is illustrated in a von Kossa-stained 5-μm thick paraffin section in Fig. 1. The section shows resting, proliferating, and hypertrophic zones of chondrocytes that define the phenotype of the tissue. Differences are apparent in the size, shape, and organization of the constituent cells, which also express a variety of genes that determine the specific function of the cells at their particular location in the growth plate. Proteins corresponding to certain of those genes may be coordinately synthesized and secreted by the same cells to form the organic extracellular component of the tissue. Individuals or groups of chondrocytes may be selected and sampled by LCM to identify and quantitate both their gene expression and protein secretion. In this study, only gene expression was examined. A series of panels comprising Fig. 2 illustrates the successful isolation of a single chondrocyte by LCM and the panels for Fig. 3 show the isolation of a portion of the constituent cells from frozen sections of the proliferating zone of the growth plate from a 9-day-old mouse tibia preserved in RNA*later*. In each of these sets of images, the region of interest within the respective growth plates is shown before and after laser capture along with the cell or cells now isolated on the polymer transfer film of Cap-Sure caps. Image comparison confirms the successful capture of chondrocytes from within the tissue section.

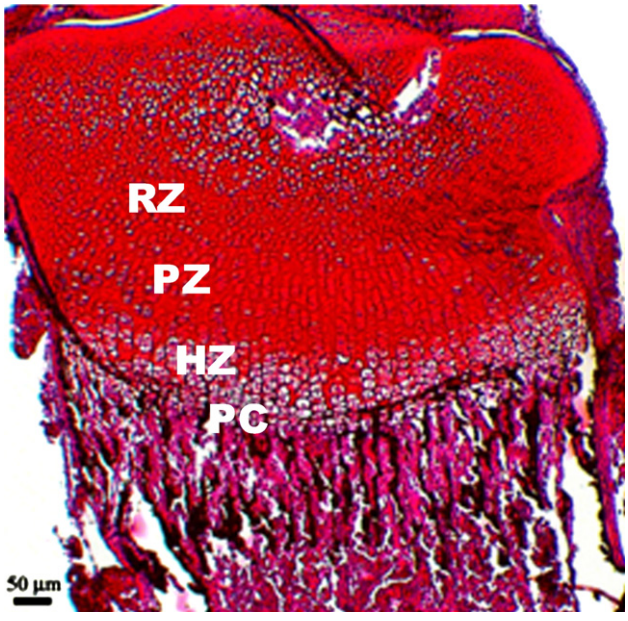

Fig. 1. Tibial epiphyseal growth plate from a 9- and 11-day-old mouse. This 5-μm section shows phenotypically distinct regions of a growth plate cartilage containing chondrocytes that may be captured by LCM and analyzed by RT-PCR as in this study. The regions illustrated are resting (RZ), proliferating (PZ), hypertrophic (HZ), and provisional calcification (PC) zones of the tissue. The specimen was fixed in paraformaldehyde, embedded in paraffin, and von Kossa-stained. The mineral phosphate stains black and is evident in the hypertrophic zone of this section. Bar, 50 μm.

Molecular analysis of laser captured cells by RT-PCR

To demonstrate gene expression from specific chondrocytes isolated from definitive regions of tibial growth plates from mice, the presence of 18S rRNA as the normalizing gene and osteopontin as an unknown gene was initially investigated. First, to confirm detection of gene expression and the quality of total RNA following the protocol described above, 18S rRNA was amplified by RT-PCR from 10 to 200 chondrocytes captured from sections of the growth plate of a normal 6-day-old B6C3F1 mouse. Gel electrophoresis (Fig. 4) compares sucrose and RNA*later* as preservatives of intact RNA from tissues. Results show that RNA*later* gave band intensities equal to or stronger than those obtained from sections of sucrose-preserved tissues for a range of 10–200 captured chondrocytes.

Subsequent experiments were conducted with cells isolated from tibial epiphyseal growth plates from 1- to 11-day-old normal B6C3F1 mice and analyzed for osteopontin expression (390 bp, Table 1) normalized to 18S rRNA. Fig. 5 verifies the presence of osteopontin expression on an ethidium bromide gel following restriction enzyme digestion of PCR amplicon with *Pvu*II. Fig. 6 presents one example of RT-PCR analysis of osteopontin expressed by chondrocytes isolated by laser capture microdissection from phenotypically distinct regions of the tibial growth plate from a 5-day-old B6C3F1 mouse. Approximately 700–1200 cells were captured from each of the zones of the tissue. Analyses of younger and older mice in a related series of growth plate studies have been

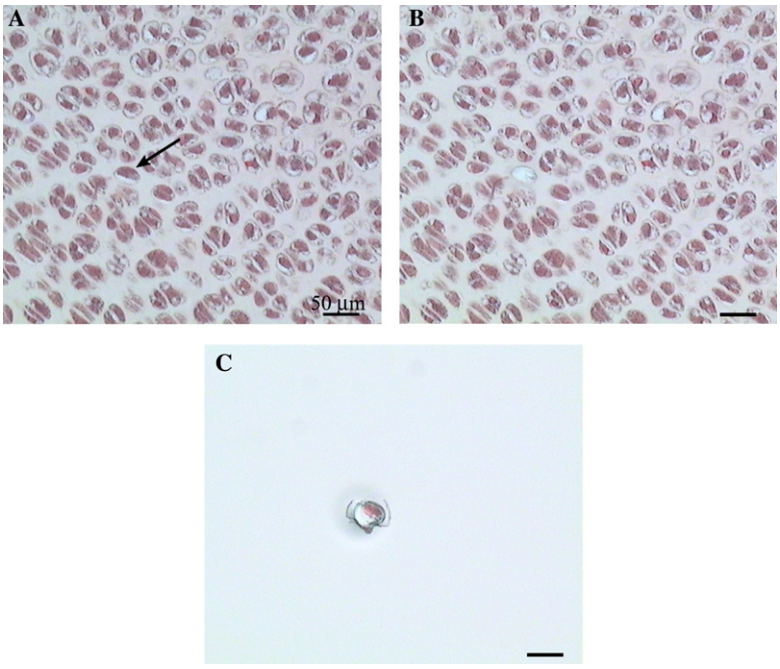

Fig. 2. Eosin-stained frozen section (5-μm thick) of epiphyseal growth plate cartilage from a 9-day-old mouse tibia demonstrating a single cell capture. The tissue is shown before (A) and after (B) laser capture microdissection of a single cell. The microdissected cell is attached to the polymer film substrate shown in (C). Bar, 50 μm for all panels.

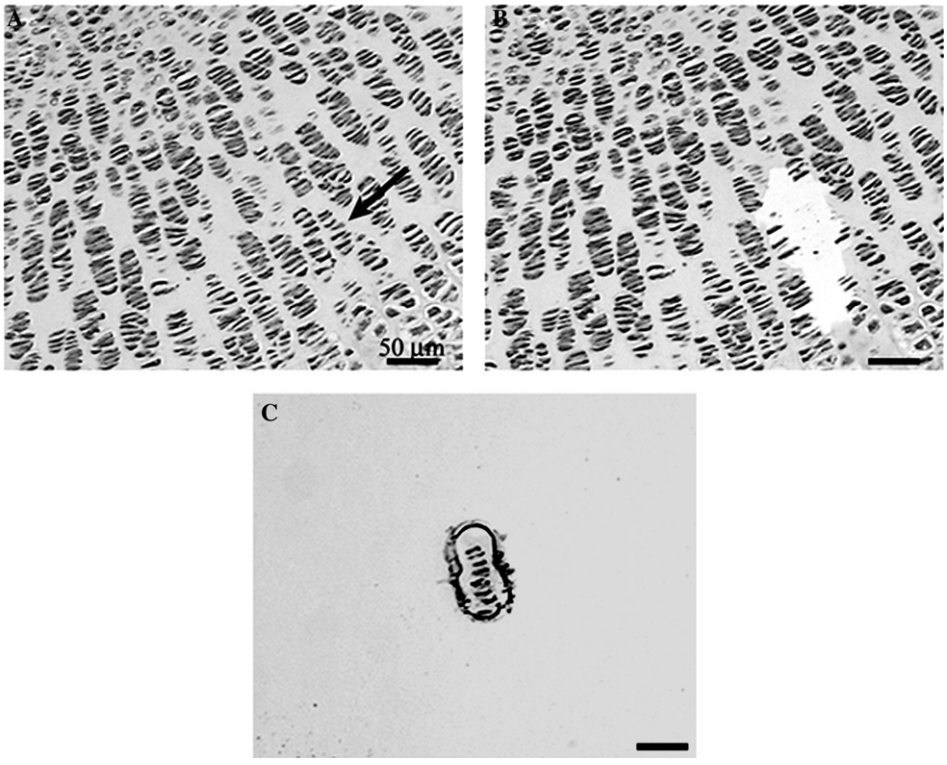

Fig. 3. Eosin-stained frozen section (5-μm thick) of epiphyseal growth plate cartilage from a 9-day-old mouse tibia demonstrating capture of a region. The tissue is shown before (A) and after (B) laser capture microdissection of a region of the proliferating zone. The microdissected zone attached to the polymer film substrate of a cap appears in (C). Bar, 50 μm for all panels.

performed and published [14]. Expression of 18S rRNA was readily detectable in all cell samples. Osteopontin was also detectable in all cells, including those from the brain of the same animal providing cartilage. Osteopontin expression varies qualitatively according to different cartilage growth plate regions.

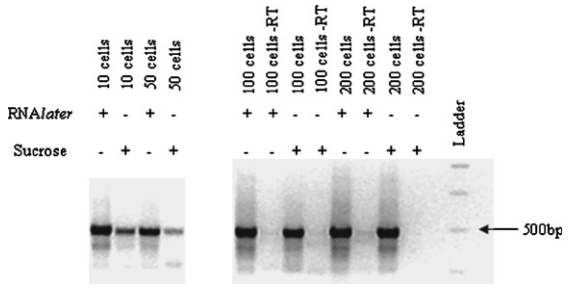

Fig. 4. Ethidium bromide gel (inverted image) of 18S rRNA (488 bp) as a marker for message preservation. Six-day-old mouse tibiae were harvested and stored in RNA*later* at −20 °C or soaked in 30% sucrose for 4 h and stored at −80 °C. Different numbers of cells (10, 50, 100, 200) were laser captured from sectioned tibia for each condition and processed for RT-PCR. Negative controls were cells captured (100, 200) and processed without the reverse transcriptase enzyme (−RT).

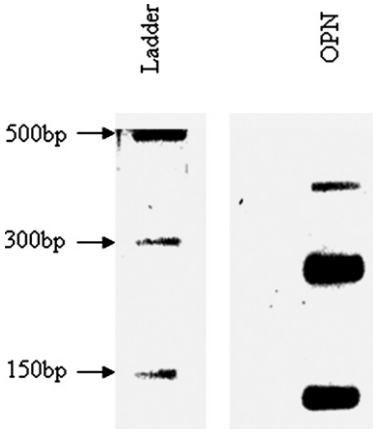

Fig. 5. Restriction digest of 390-bp amplicon generated from murine OPN primers. The PCR product was excised from a 2% agarose gel, purified and cut with *Pvu* II (Takara Mirus Bio) for 1 h at 37 °C. The reaction products were visualized on a 3% ethidium-bromide-stained agarose gel (inverted image). *Pvu*II has one restriction site in the 390-bp OPN sequence and yields two fragments of 260 and 130 bp. This gel shows that the majority of the 390-bp product generated from the OPN primers is cut into two fragments of the correct molecular weight by *Pvu*II as a confirmation of the OPN PCR product.

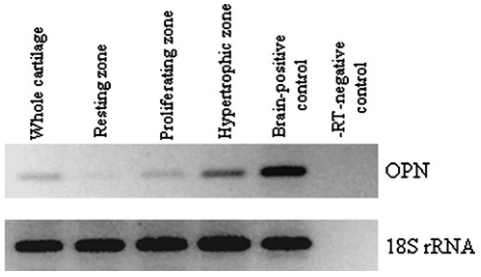

Fig. 6. Ethidium bromide gel (inverted image) of RT-PCR of OPN and 18S rRNA from 200 to 300 chondrocytes captured from the whole growth plate cartilage and the resting, proliferating, and hypertrophic regions of growth plates from 5-day-old mice. Brain cells from an animal of the same age and a reaction without reverse transcriptase (−RT) were used as respective positive and negative controls. Normalized to 18S rRNA, OPN shows a qualitative increase from resting to hypertrophic regions.

While there are clear differences in osteopontin expression evidenced in gels such as shown in Fig. 6, and such expression can be normalized to an 18S rRNA standard, it remains difficult to determine quantitative changes in osteopontin using an end point analysis of the type represented in this example. In this case, subsequent measures of osteopontin or gene expression in general were performed using real-time QRT-PCR. Laser capture microdissection was again applied to isolate specific cell populations and RNA from tibial growth plate cartilage, in this instance from a normal 9-day-old B6C3F1 mouse (Fig. 1). For these QRT-PCR studies, mouse-specific primers were designed for osteopontin, aggrecan, and 18S rRNA (Table 1). Standard curves generated from serial dilutions of mouse control cDNA that are shown in Fig. 7 have linear correlation coefficient (R^2) values of 0.99. The validation curves, as described under Materials and Methods, for osteopontin and 18S rRNA and for aggrecan and 18S rRNA showed that the absolute values of the slopes were 0.13 and 0.12, respectively. The dissociation curves for the amplified products gave a single peak corresponding to a specific melting temperature (Fig. 8) and the products detected on an agarose gel showed a single band at the correct molecular weight (data not shown).

After validation of the primer sets of interest, the cDNA pool generated from the RT reaction of the mouse growth plate zones (resting, proliferating, and hypertrophic; see Figs. 1 and 3) was divided and the samples were run in triplicate for each primer set. Table 2 presents the results of osteopontin and aggrecan analysis in this growth plate example. Average and standard deviations of C_T values obtained from the PCR and the fold difference in expression determined using the comparative C_T method [20] are shown. As noted under Materials and methods, the ΔC_T is the C_T of the target gene normalized to the C_T of the reference gene, in this case 18S rRNA. The expression levels of captured chondrocytes comprising resting and hypertrophic zones of cartilage were compared to the expression levels of captured cells from the proliferating zone, arbitrarily chosen as the calibrator and set to a value of 1.0 [20]. Osteopontin (OPN_N) normalized to 18S rRNA from chondrocytes of the hypertrophic and resting zones showed approximately a 5-fold increase over cells from the proliferating zone in the 9-day-old mouse (Table 2). Normalized aggrecan (AGG_N) from resting and hypertrophic zone chondrocytes showed approximately 1.5- and 3-fold decreases, respectively, compared to captured proliferating zone cells in the 11-day-old animal (Table 2).

Negative controls were run for quality assurance and consisted of the −RTs, NTCs, and buffer blanks as outlined under Materials and methods. Analyses of the SYBR Green buffer blank yielded consistent C_T values of 40 (no contamination). The −RTs, NTCs, and buffer

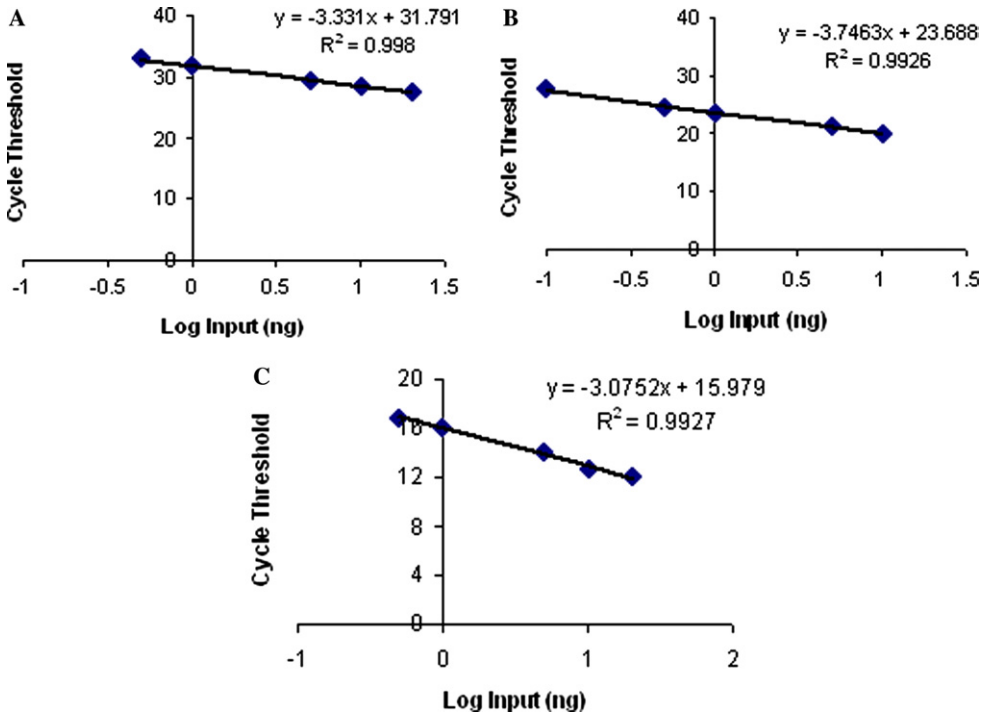

Fig. 7. Relative standard curves generated from serial dilutions of mouse bone cDNA. (A) Aggrecan, (B) OPN, and (C) 18S rRNA primers were used to amplify ~0.1 to 20 ng of cDNA that was reverse transcribed from total RNA isolated from mouse bone. The average C_T values (cycle threshold) are plotted against the logarithm (base 10) of the input amount of cDNA.

blanks for osteopontin also gave C_T values of 40. The −RTs, NTCs, and buffer blanks for aggrecan gave C_T values averaging between 36 and 37, attributable to small primer dimer formation as noted in the melting curve analysis of these samples (data not shown). The –RTs, NTCs, and buffer blanks for 18S rRNA had an average C_T value of 33.

Discussion

The protocol outlined here has been presented and optimized for the laser capture microdissection of chondrocytes from a mineralizing tissue, in this particular case, that of fresh-frozen sections of the mineralizing cartilaginous epiphyseal growth plates from mouse tibiae. An Arcturus PixCell II was utilized for chondrocyte isolation. Further, the methodology has been designed to recover RNA from hard tissues for subsequent gene analysis leading to quantitative real-time PCR. The advantage of LCM coupled with PCR is procuring a homogeneous population of cells, numbering from 1 to 1000s or more, that can be analyzed for gene expression. This coupling of LCM and PCR is critical for obtaining and evaluating the expression profile of a specific cell type or subpopulation of cells rather than that of different cell types comprising heterogeneous populations [21–24]. Problems associated with precise gene analysis have commonly concerned the means for successful isolation of high quality RNA. Integrity of RNA leads to both accurate gene expression profiles and reproducible experiments. The assurance of high quality intact RNA was an integral part of this study.

Varieties of laser capture or assisted microdissection systems are continuing to be developed and improved [18,22,23]. The Arcturus PixCell II system utilizes the NIH patent of a near-infrared laser pulse that melts a thermoplastic ethylene vinyl acetate transfer film around the cells of interest in a tissue section [3,25]. The film, as noted under Materials and methods, covers the end of a small cap that is placed on the flat, dry section. Functionally, the laser raises the temperature of the film at its focal point on the film. The transfer film absorbs laser energy and subsequently melts into the interstitial spaces of the section, which lies beneath and maintains very close contact with the film [3]. The bond formed in this manner between the tissue section and the transfer film is stronger than that between the section and glass slide on which it is mounted, and the cells, now essentially annealed to the film, can be lifted directly from the section with a mechanical arm. Because the laser energy is poorly absorbed by cells, nucleic acids or proteins are not degraded [3,25]. The cap, holding the transfer film with captured cells or matrix regions of interest, is then inserted into the end of an Eppendorf tube containing extraction buffer as noted under Materials and methods previously. Other microdissection systems may not require a flat, dry tissue section like the Arcturus instrument used in this study. Instead, these employ a laser

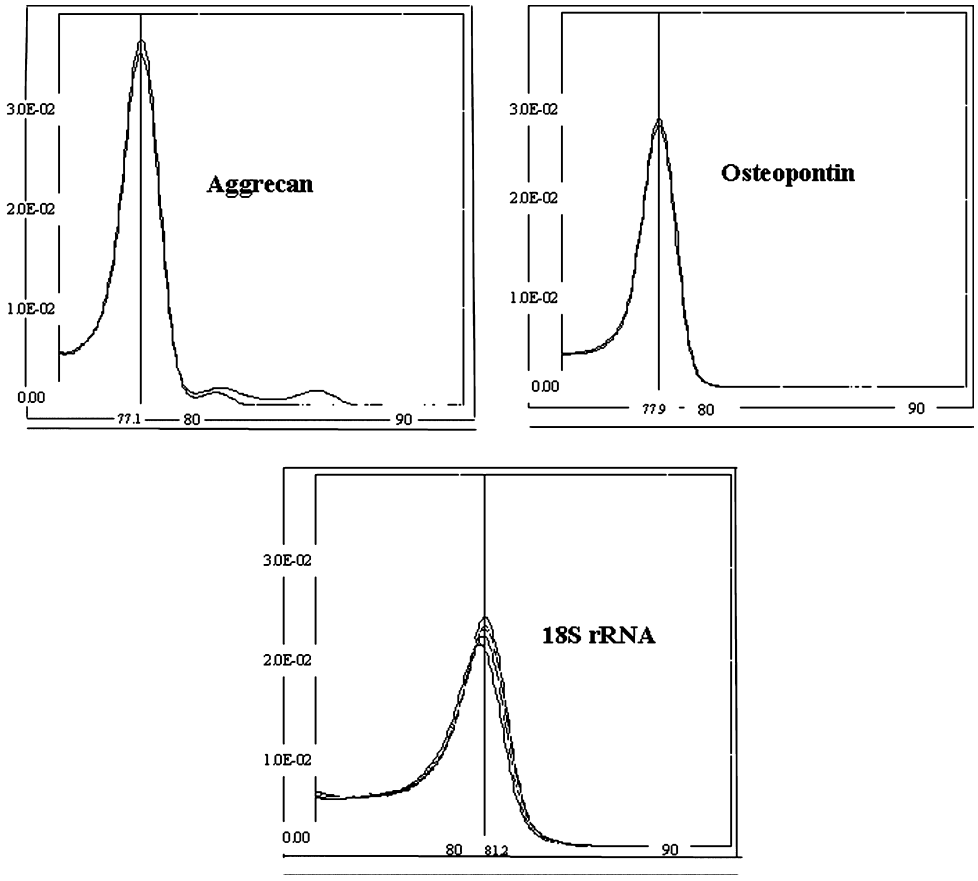

Fig. 8. Melting curve analysis of PCR products generated from aggrecan, OPN, and 18S rRNA primers. Graphs shown are plotted from the dissociation curve analysis software v1.ob1 (Applied Biosystems). When the PCR cycles are complete, the products are slowly melted and the fluorescence is recorded as it decreases with increasing temperature. The first derivative of the fluorescence from the melting curve analysis is plotted against increasing temperature and the peak represents the melting temperature (T_m) of the product, which should closely correspond to the calculated melting temperature for the product. Aggrecan has a T_m of 77.1 °C, OPN has a T_m of 77.9 °C, and 18S rRNA has a T_m of 81.2 °C.

Table 2
Expression of osteopontin and aggrecan in mouse resting, proliferating, and hypertrophic zones using the comparative C_T method

Tissue zones (9-day-old mouse)	OPN average C_T	18S average C_T	ΔC_T (OPN-18S)	$\Delta\Delta C_T$ ($\Delta C_T - \Delta C_T$ proliferating zone)	OPN_N relative to proliferating[a]
Expression of osteopontin					
Resting	31.61 ± 0.42	14.08 ± 0.08	17.53 ± 0.43	-2.38 ± 0.43	5.2 (3.9–7.0)
Proliferating	35.54 ± 0.57	15.63 ± 0.06	19.91 ± 0.57	0.00 ± 0.57	1.0 (0.7–1.5)
Hypertrophic	32.00 ± 0.27	14.30 ± 0.01	17.70 ± 0.27	-2.21 ± 0.27	4.6 (3.8–5.6)
Tissue zones (11-day-old mouse)	AGG average C_T	18S average C_T	ΔC_T (AGG-18S)	$\Delta\Delta C_T$ ($\Delta C_T - \Delta C_T$ proliferating zone)	AGG_N relative to proliferating[a]
Expression of aggrecan					
Resting	30.68 ± 0.25	18.45 ± 0.40	12.23 ± 0.47	0.62 ± 0.47	0.7 (0.5–0.9)
Proliferating	28.45 ± 0.06	16.84 ± 0.27	11.61 ± 0.28	0.00 ± 0.28	1.0 (0.8–1.2)
Hypertrophic	29.72 ± 0.21	16.41 ± 0.02	13.32 ± 0.21	1.71 ± 0.21	0.3 (0.3–0.4)

[a] The OPN_N and AGG_N relative to the proliferating zone are calculated using the equation $2^{-\Delta\Delta C_T}$, with the range determined by $\Delta\Delta C_T$ plus the standard deviation and $\Delta\Delta C_T$ minus the standard deviation.

that cuts around the periphery of a specimen area, allowing cells or matrix regions of interest to drop or be transferred by hand into the buffer tubes. Discussion of aspects of laser capture instruments other than the Arcturus PixCell II is beyond the scope of this paper.

There are a number of important considerations with regard to successful laser capture and subsequent gene analysis of mineralized material. The following paragraphs address them and include many unpublished qualitative observations that contributed to optimizing

methodology. With respect to the preparation of tissue for individual cell isolation, it is critical to produce dry and flat sections. Both of these features are required for proper laser melting of the transfer film to the tissue and for consistent grabbing and pulling the cells or matrix regions of interest from sections. Dry sections are routinely obtained through use of graded ethanols and a final xylene dip of the glass slides. The procedure (http://dir.nichd.nih.gov/lcm/lcm.htm) is well documented and was adapted for this study. To generate a flat intact section from undecalcified mineralizing tissue is a more daunting task than producing a dry section and requires experience and patience. In the present methodology, parameters were varied in the preservation of the tissues to generate frozen sections with paraffin-like quality. The combination of RNA*later* and the CryoJane Tape Transfer System was found to produce tissue sections of consistent quality necessary to perform LCM with adjustments in the strength and duration of the laser pulse to achieve capture of desired cells. The processing of slides and section fixation, staining, and dehydration also had an effect on the quality of sections and the amount and condition of RNA recovered from captured cells. In this context, it is important to consider some aspects of these approaches.

Preserving whole samples in RNA*later* was found to be extremely advantageous in that they were stored subsequently at −20 °C, circumventing the necessity otherwise of processing and sectioning specimens immediately to prevent RNA alteration. Storage at −20 °C could be continued for a relatively long time but not indefinitely for mineralized tissues. The storage period used in these studies was less than 1 year before changes were noted in RNA integrity. Specimen storage at −20 °C, rather than at a much lower temperature such as −80 °C for maintaining RNA integrity, prior to sectioning at −20 °C held another advantage. The fact that storage and sectioning were performed at the same temperature prevented brittle and fractured tissue on cryostat sectioning, a characteristic that frequently occurs when specimens are brought to −20 °C from −80 °C.

The CryoJane Tape Transfer System was indispensable for producing flat sections of mineralized tissues, which consist of both organic and inorganic matrices that behave differently on sectioning. One of the variables found here in utilizing the CryoJane was the temperature of cryosectioning. In this regard, a rather narrow range between −20 and −30 °C gave optimal results and, in many cases, adjustments toward −30 °C were preferable. Cryosectioning temperature, however, was not the single determinant of success with tissue processing. A major concern was also the resulting morphology of a section. To investigate optimizing the structural integrity of sections, harvested bone tissue was initially treated in different ways. In addition to its immersion in RNA *later* and storage at −20 °C as described above under Materials and methods, bone tissue was snap-frozen in liquid nitrogen or in isopentane cooled in liquid nitrogen and stored at −80 °C; it was soaked for 4 h in 30% sucrose at 4 °C and stored at −80 °C; or it was embedded in Tissue Freezing Medium (Triangle Biomedical Sciences, Durham, NC), Histoprep Frozen Tissue Embedding Media (Fisher, Pittsburgh, PA), or CryoGel (Instrumedics, Hackensack, NJ) in ice cube trays with −80 °C storage. None of these techniques was found to give suitable tissue morphology following retrieval of the specimens from −80 °C and then cryosectioning at −20 °C. As noted above, it appears that storage at −80 °C and transition to −20 °C were problematic, resulting in sections that were brittle, rippled, or incomplete. Bone samples stored at −20 °C in RNA*later* and subsequently sectioned at −20 to −30 °C yielded the most intact sections having optimal organic and inorganic structure. Fortunately, then, −20 °C was useful for both ease of cryosectioning and production of optimal tissue morphology.

The CryoJane Tape Transfer System utilizes adhesive-coated glass slides to help assure flat sections of tissue following cryomicrotomy. The slides are currently available with three different degrees of adhesiveness (1/2×, 1×, and 4×). The study here determined that 1/2× or 1× slides were satisfactory for sections of mineralized tissue, but 4× slides, which provide increased adhesion on UV polymerization, produced incomplete fractured sections. The use of 1/2× and 1× slides is far superior to the use of noncoated clean glass for achieving flat sections relatively free of wrinkles, tears, and related features.

As one factor, the adhesiveness of CryoJane slides may affect the laser capture of individual cells from mounted sections. Adherence may be so tight that cells can be captured only inconsistently or not at all or so ineffectively that large numbers of unwanted cells or excess matrix regions are lifted from a section with the mechanical arm of the PixCell II unit. Thus, testing of 1/2×, 1×, and 4× slides is necessary to determine the appropriate choice, and this in turn requires study of laser power conditions that optimize cell isolation. In this regard, it was found that 70–80 mW power and 1.5–2.5 ms pulse duration gave excellent results of single chondrocyte capture in this study. Any extraneous cells or debris collected on a cap were removed easily by gently touching the cap to the clean sticky surface of a Post-it or Highland note or Scotch double-coated tape (Minnesota Mining and Manufacturing, St. Paul, MN). The choice of laser power and duration depended on the dryness of the mounted section and as a result was variable from one group of slides to another. Ideally, the proper power to melt the polymer and the proper pulse duration to remove and isolate individual cells from their sections were selected. This and other procedures in the process of laser capture involved trial and error testing of the power and duration parameters.

The processing of a mounted section through fixation, staining, and dehydration also affects cell capture. This aspect of the technique again involves the degree of wetness of a section, which ideally should be eliminated or minimized as completely as possible. Any moisture present in a section will interfere adversely with the interaction between the tissue and the polymer transfer film of a cap, making cell or matrix capture variable or unsuccessful. To mediate this result, the initial processing of mounted frozen sections is their transfer to ethanol inside a −80 °C freezer. This step has been found in the present study to ensure much more reliable capture than allowing sections to thaw at room temperature, even for brief periods, before placing them in ethanol solution. Subsequently, the sections are routinely dehydrated through further graded ethanols and xylene. Staining prior to the final xylene steps is accomplished in alcoholic eosin and the sections are then stored in a desiccator over Drierite until laser capture.

Following measures to preserve the integrity of sample RNA, including use of DEPC-treated water for all solutions, reverse transcription reactions were optimized for consistency and reproducibility. In this regard, conditions were chosen from the literature or determined empirically to make such reactions as efficient as possible, that is, to approximate a cDNA:RNA ratio of 1:1 [21]. In the event of partial degradation of RNA, the cDNA yield from sequences near its 5′ end is known to be significantly less than that from sequences near its poly(A) tail with the use of oligo(dT) primers [26]. Thus, both random hexamers and oligo(dT) primers were used in reverse transcription reactions so as not to skew the cDNA yield in favor of 3′ ends and to represent more accurately all sequences of the RNA population. In addition, products are available to decrease processing time and reduce operator handling and possible contamination by combining the reverse transcription and PCRs in a single tube. However, a two-tube/two-enzyme-based approach, although inconvenient, was found in this study to be more sensitive for product amplification than the one-tube methodology. This observation has also been reported elsewhere [21,27]. It is possible that enzymes from different manufacturers may affect maximizing reverse transcription products [21]. In the present study, reverse transcriptase or DNA polymerase enzymes from Applied Biosystems were exclusively utilized with the Applied Biosystems instrumentation available in this laboratory.

Traditional PCR methods rely on end point analysis and are therefore at best semi-quantitative. Initially, gel electrophoresis was used to examine PCR products to determine gene expression. This method of post-analysis is indirect as it relies on the stain intensity of the gene products rather than the products themselves. Furthermore, detection and measurement of stain intensity are subject to potential gel-to-gel, operator, and instrumentation inconsistencies. While limited, then, in its application, gel electrophoresis was valuable in this study as a means for qualitatively screening differences and optimizing conditions for gene expression profiling. In this regard, the data from 5-day-old mice (Fig. 6) show qualitative differences in OPN expression over their various growth plate zones. In an attempt to make these analyses more quantitative, competitive templates were included with 18S rRNA, in this case copetimers from Ambion. The procedure, however, was laborious and challenging and did not necessarily yield reliable or reproducible results. As a consequence, copetimers were not utilized and real-time RT-PCR was ultimately employed. Indeed, QRT-PCR has several advantages over other traditional gene analysis methods [21,28].

The processing of tissues and the isolation of cells by LCM may lead to degradation of RNA. QRT-PCR of LCM tissue that may be less than optimal, containing partially degraded RNA, has another advantage over alternative PCR-based methods in that the size of amplified products typically ranges from 60 to 90 bp for real time instead of larger 200- to 300-bp amplicons typically designed in other approaches. As an example, the isolation of RNA from paraffin-embedded tissues and the subsequent quantitation of gene expression have had some success for relatively small amplicon size. Specht et al. [29] divided specimens and processed them as either frozen or paraffin-embedded samples prior to QRT-PCR for comparison of increasing amplicon length. Results showed that up to an amplicon length of 100 bp, both processing methods yielded equivalent levels of gene expression, but, beyond 100-bp size, paraffin-embedded samples were greatly reduced in expression compared to frozen. This observation was attributable to the degradation of RNA in the paraffin process [29]. The important point illustrated by this set of experiments is that QRT-PCR is extremely useful for less than optimal RNA and it is especially valuable when coupled to LCM tissues as done in the present work.

Another consideration in the context of QRT-PCR analysis is the choice and use of an appropriate detection method. Presently, SYBR Green, Taqman, and molecular beacons are commonly utilized as a fluorescent dye or probe. The design, synthesis, optimization, and respective advantages of these detection formats have been recently reviewed in detail [21,28]. In a related context, the selection of 18S rRNA as an appropriate control for normalization in the QRT-PCR assay was based on its invariance compared to other possible controls [21,28]. In addition, since LCM sample size falls typically into nanogram ranges, genomic DNA contamination becomes problematic. For this reason, DNase treatment of total RNA isolates was applied with excess enzyme for 2 h in these studies. NTCs and buffer blanks were always included in every QRT-PCR assay to verify the absence of any potential contaminating PCR product.

Statistical analysis of gene expression is an important subject in the context of QRT-PCR, and the choice of an appropriate statistical methodology depends on the specifics of a given experimental protocol. For the present work, of the three available statistical approaches with the ABI 7700, there is equivalency in the use of an absolute standard curve, relative standard curve, and comparative C_T methods [30]. The latter was the method of choice here, based simply on cost consideration.

The particular example presented here for a growth plate from a 9- and 11-day-old mouse shows specific quantitative expression levels for cells isolated by LCM. Such values for OPN and aggrecan related so directly to the various zones of a growth plate for mouse or any other animal have not been obtained previously. Thus, these quantitative data may begin to establish the biological pattern of expression of these two genes spatially correlated with growth plate structure. Clearly, additional studies with other genes will be extremely valuable in this structural context and can be extended to examine temporal changes in growth plate genes from animals of different ages.

It should be noted that the quantitative results given here (Table 2) differ from qualitative screening (Fig. 6) in that the pattern of gene expression correlated with growth plate zones is not identical. This is as expected since qualitative information is not definitive and must be verified by quantitative methods and since these two examples represent mice of different ages. On the other hand, it may be that the qualitative and quantitative results are both accurate since the pattern of expression of OPN and aggrecan, as they relate to individual growth plate zones, would undoubtedly change as a function of the age and maturation of the chondrocytes comprising the tissue. In any case, the qualitative and more specific quantitative data each support the accepted biological concept that chondrocytes from different growth plate regions maintain functional distinction, in part attributable to differences in their respective gene expression levels.

In summary, then, this paper provides details for the use of LCM coupled with either RT-PCR or QRT-PCR to examine the expression of certain genes found in cell populations comprising the murine tibial epiphyseal growth plate. The methodologies described are intended to help guide further work of this and other mineralizing vertebrate connective tissues in the direction of valuable structure/function relationships.

Acknowledgments

This work was supported by National Institutes of Health Grant AR41452 (to WJL). The authors thank Jean Zhang (Department of Physiology and Pharmacology, Northeastern Ohio Universities College of Medicine) for her technical assistance.

References

[1] M.R. Emmert-Buck, R.F. Bonner, P.D. Smith, R.F. Chauqui, Z. Zhuang, S.R. Goldstein, R.A. Weiss, L.A. Liotta, Laser capture microdissection, Science 274 (1996) 998–1001.
[2] E. Trogan, R.P. Choudhury, H.M. Dansky, J.X. Rong, J.L. Breslow, E.A. Fisher, Laser capture microdissection analysis of gene expression in macrophages from atherosclerotic lesions of apolipoprotein E-deficient mice, Proc. Natl. Acad. Sci. USA 99 (2002) 2234–2239.
[3] R.F. Bonner, M.R. Emmert-Buck, K. Cole, T. Pohida, R.F. Chauqui, S.R. Goldstein, L.A. Liotta, Laser capture microdissection: molecular analysis of tissue, Science 278 (1997) 1481–1483.
[4] S.M. Goldsworthy, P.S. Stockton, C.S. Trempus, J.F. Foley, R.R. Maronpot, Effects of fixation on RNA extraction and amplification from laser captured microdissected tissue, Mol. Carcinogen. 25 (1999) 86–91.
[5] F. Noack, D. Helmecke, R. Rosenberg, S. Thorban, H. Nekarda, U. Fink, J. Lewald, M. Stich, K. Schutze, N. Harbeck, V. Magdoen, H. Grasff, M. Schmitt, CD87-positive tumor cells in bone marrow aspirates identified by confocal laser scanning fluorescence microscopy, Int. J. Oncol. 15 (1999) 617–623.
[6] M. Kremer, M. Spitzer, S. Mandl-Weber, K. Stecker, B. Schmidt, H. Hofler, L. Quintanilla-Martinez, F. Fend, Discordant bone marrow involvement in diffuse large B-cell lymphoma: comparative molecular analysis reveals a heterogeneous group of disorders, Lab. Invest. 83 (2003) 107–114.
[7] M. Hoffman, K. Olson, A. Cavender, R. Pasqualini, J. Gaikwad, R.N. D'Souza, Gene expression in a pure population of odontoblasts isolated by laser-capture microdissection, J. Dent. Res. 80 (2001) 1963–1970.
[8] M. Hoffman, J. Gaikwad, G. Schmalz, A. Cavender, R.N. D'Souza, Analysis of odontoblast gene expression using a novel approach, laser capture microdissection, Connect. Tissue Res. 43 (2002) 376–380.
[9] C.S. Young, S. Terada, J.P. Vacanti, M. Honda, J.D. Bartlett, P.C. Yelick, Tissue engineering of complex tooth structures on biodegradable polymer scaffolds, J. Dent. Res. 81 (2002) 695–700.
[10] W.J. Landis, J. Zhang, R. Jacquet, Gene expression from single chondrocytes isolated by laser capture microdissection of vertebrate bone, FASEB J. 14 (2000) A1470.
[11] W.J. Landis, J. Zhang, R. Jacquet, Gene expression of isolated individual chondrocytes from growth plate cartilage, Am. Soc. Bone Miner. Res. 15 (2000) S206.
[12] W.J. Landis, R. Jacquet, J. Hillyer, J. Zhang, Insight into the role of osteopontin deduced from laser capture microdissection of mouse growth plate cartilage, J. Bone Miner. Res. 16 (2001) S236.
[13] R. Jacquet, J. Hillyer, J. Zhang, W.J. Landis, Application of novel laser capture microdissection and RT-PCR to a functional analysis of osteopontin in mouse growth plate cartilage, Microsc. Microanal. 7 (2001) 44–45.
[14] W.J. Landis, R. Jacquet, J. Hillyer, J. Zhang, Analysis of osteopontin in mouse growth plate cartilage by application of laser capture microdissection and RT-PCR. Chemistry and biology of mineralized tissue, Connect. Tissue Res. 44 (2003) 1–5.
[15] J.-O. Kim, H.-N. Kim, M.-H. Hwang, H.-I. Shin, S.-Y. Kim, R.-W. Park, E.-Y. Park, I.-S. Kim, A.J. van Wijnen, J.L. Stein, J.B. Lian, G.S. Stein, J.-Y. Choi, Differential gene expression analysis using paraffin-embedded tissues after laser microdissection, J. Cell. Biochem. 90 (2003) 998–1006.

[16] T. Scharschmidt, R. Jacquet, J. Hillyer, S. Weiner, P. Flanagan, W.J. Landis, RNA retrieval from frozen and archival osteoarthritic tissue utilizing laser capture microdissection, J. Bone Miner. Res. 16 (2001) S235.
[17] R. Parlato, A. Rosica, V. Cuccurullo, L. Mansi, P. Macchia, J. Owens, J.F. Mushinski, M. De Felice, R.F. Bonner, R. Di Lauro, A preservation method that allows recovery of intact RNA from tissues dissected by laser capture microdissection, Anal. Biochem. 300 (2002) 139–145.
[18] C.A. Suarez-Quian, S.R. Goldstein, T. Pohida, P.D. Smith, J.I. Peterson, E. Wellner, M. Ghany, R.F. Bonner, Laser capture microdissection of single cells from complex tissues, BioTechniques 26 (1999) 328–335.
[19] K.M. Ririe, R.P. Rasmussen, C.T. Wittwer, Product differentiation by analysis of DNA melting curves during the polymerase chain reaction, Anal. Biochem. 245 (1997) 154–160.
[20] User Bulletin #2: ABI PRISM 7700 Sequence Detection System, PE Applied Biosystems, Foster City, CA, 1997.
[21] S.A. Bustin, Quantification of mRNA using real-time reverse transcription PCR (RT-PCR): trends and problems, J. Mol. Endocrinol. 29 (2002) 23–39.
[22] N.L. Simone, R.F. Bonner, J.W. Gillespie, M.R. Emmert-Buck, L.A. Liotta, Laser-capture microdissection: opening the microscopic frontier to molecular analysis, Trends Genet. 14 (1998) 272–276.
[23] Y. Sirivatanauksorn, R. Drury, T. Crnogorac-Jurcevic, V. Sirivatanauksorn, N.R. Lemoine, Laser-assisted microdissection: applications in molecular pathology, J. Pathol. 189 (1999) 150–154.
[24] K. Suzuki, H. Matsui, M. Hasumi, Y. Ono, H. Nakazato, H. Koike, K. Ito, Y. Fukabori, K. Kurokawa, H. Yamanaka, Gene expression profiles in human BPH: utilization of laser-capture microdissection quantitative real-time PCR, Anticancer Res. 21 (2001) 3861–3864.
[25] S.R. Goldstein, P.G. McQueen, R.F. Bonner, Thermal modeling of laser capture microdissection, Appl. Opt. 37 (1998) 7378–7391.
[26] G.H. Swift, M.J. Peyton, R.J. MacDonald, Assessment of RNA quality by semi-quantitative RT-PCR of multiple regions of a long ubiquitous mRNA, BioTechniques 28 (2000) 524–531.
[27] M. Battaglia, P. Pedrazzoli, B. Palermo, A. Lanza, F. Bertolini, N. Gibelli, G.A. Da Prada, A. Zambelli, C. Perotti, G. Robustelli della Cuna, Epithelial tumour cell detection and the unsolved problems of nested RT-PCR: a new sensitive one step method without false positive results, Bone Marrow Transplant. 22 (1998) 693–698.
[28] S.A. Bustin, Absolute quantification of mRNA using real-time reverse transcription polymerase chain reaction assays, J. Mol. Endocrinol. 25 (2000) 169–193.
[29] K. Specht, T. Richter, U. Muller, A. Walch, M. Werner, H. Hofler, Quantitative gene expression analysis in microdissected archival formalin-fixed and paraffin-embedded tumor tissue, Am. J. Pathol. 158 (2001) 419–429.
[30] M.R. Johnson, W. Kangsheng, J.B. Smith, M.J. Heslin, R.B. Diasio, Quantitation of dihydropyrimidine dehydrogenase expression by real-time reverse transcription polymerase chain reaction, Anal. Biochem. 278 (2000) 175–184.